Active Reaction Sites for Oxygen Reduction in $La_{0.9}Sr_{0.1}MnO_3$/YSZ Electrodes

Hee Y. Lee, Woo S. Cho, and Seung M. Oh*

Department of Chemical Technology, College of Engineering, Seoul National University, Seoul 151-742, Korea

H.-D. Wiemhöfer[a] and W. Göpel

Institute for Theoretical and Physical Chemistry, University of Tübingen, D-72076 Tübingen, Germany

ABSTRACT

Active reaction sites for O_2 reduction in $La_{0.9}Sr_{0.1}MnO_3$ electrode have been characterized by addressing the origin of the cathodic polarization effects on this electrode material. Cathodic polarization (up to −1.2 V *vs.* Pt reference electrode) had several effects on O_2 reduction kinetics. First, the O_2 reduction rate was favorably increased when the perovskite electrode was cathodically polarized. Second, *in situ* x-ray photoelectron spectroscopy results indicated that the Mn ions are electrochemically reduced and concomitantly the oxygen stoichiometry decreases. Reduction of Mn ions was further demonstrated in the cyclic voltammogram traced under nitrogen atmosphere. Third, hysteresis in cathodic currents was observed in the cyclic voltammograms of the perovskite/YSZ/Pt system, and the hysteresis phenomena were more prominent at higher O_2 pressure. We interpreted these findings to mean that the internal and/or external surface oxide vacancies participate in the O_2 reduction reaction. However, it has been explained from the P_{O_2}-dependent hysteresis phenomena that, even though those surface sites are active in the O_2 reduction, their activity is less than that of the three-phase boundary sites since additional diffusional processes are required for the former sites. Consequently, the three-phase boundary sites are the major reaction sites at lower O_2 pressure, which leads to a small hysteresis. However, at higher O_2 pressure, the surface sites also participate in the reaction, resulting in a larger hysteresis.

Strontium-doped lanthanum manganites ($La_{1-x}Sr_xMnO_3$) are widely studied for their possible applications as cathode materials in solid oxide fuel cell systems.[1-3] Even though many results have been reported on aspects of the oxygen reduction kinetics and on the nature of the active reaction sites, there still remain controversies on this issue in the literature.[4-8]

The manganite perovskites are electronic conductors,[9] but under cathodic potential they are supposed to be partially reduced, creating oxide vacancies.[6,10,11] Rate enhancement found in cathodically polarized electrodes has been interpreted with an assumption that surface oxide vacancies are active for oxygen reduction.[5,6] Another set of the previous results that oxygen reduction kinetics can be improved by Sr doping to $LaMnO_3$ has also been explained with the same assumption.[5,6]

On the contrary, other reports suggested that the surface sites cannot participate in O_2 reduction since the O^{2-} bulk diffusion in the manganites is negligible compared to the cobalt analogs or YSZ electrolytes.[12] The favorable effect of the cathodic polarization was also attributed to the enlargement of the three-phase boundary lines.[7,13] It is likely, however, that the surface or grain boundary diffusion in porous electrodes cannot totally be discarded for their possible contribution to the overall kinetics since in general surface or grain boundary diffusion is much faster than bulk diffusion.

In this study, we tried to elucidate the nature of the active sites for O_2 reduction and the origin of the favorable effects of the cathodic polarization. To this end, *in situ* x-ray photoelectron spectroscopy was utilized to see whether oxide vacancies are produced on the surface of the cathodically polarized electrodes and also, to see whether the surface oxide vacancies actually participate in O_2 reduction, electrochemical techniques such as cyclic voltammetry and ac impedance spectroscopy were employed.

Experimental

Materials.—Aqueous solutions of nitrate of La, Sr, and Mn were mixed together in the proper molar ratio, into which an excess amount of citric acid (1.2 times of the equivalent) was added. The resulting solution was then concentrated to give viscous sol and further dried under vacuum to give a gel. The gel was crushed and calcined at 800°C for 5 h. The resulting powder was milled for 12 h in ethyl alcohol using zirconia media. The final powder product was obtained after screening with 400 mesh standard sieve. X-ray powder diffraction analysis of the product indicated a perovskite structure with no discernable impurities.[5] The particle size distribution is shown in Fig. 1. About half of the powder has a particle size of 1 μm.

Deposition of electrodes.—The powder was dispersed in turpentine oil and silk-printed (400 mesh) on the polycrystalline 8 mole percent (m/o) YSZ disk (diameter = 1.8 cm, thickness = 1 mm). Sintering was performed at 1200°C for 6 h. As a counter- and reference electrode, Pt paste (Ferro No. 4082) was silk-printed (100 mesh) on the other side of the disk and sintered at 950°C for 1 h. The areas of the working, counter-, and reference electrodes were 0.22, 1.17, and 0.15 cm^2, respectively.

For the electrical contact, a piece of Pt gauze was contacted on the cathode surface and pressed with an alumina tube. For the counter- and reference electrode, Pt wires were attached on the electrodes with Pt paste.

Electrochemical measurements.—The cell was located inside of the furnace, and the oxygen partial pressure was controlled by mixing a proper ratio of nitrogen and oxygen. The actual O_2 pressure was measured with an oxygen sensor prepared with a zirconia tube and Pt paste. The total flow rate was controlled to have 150 cm^3/min. Electrochemical measurements were performed with the three-

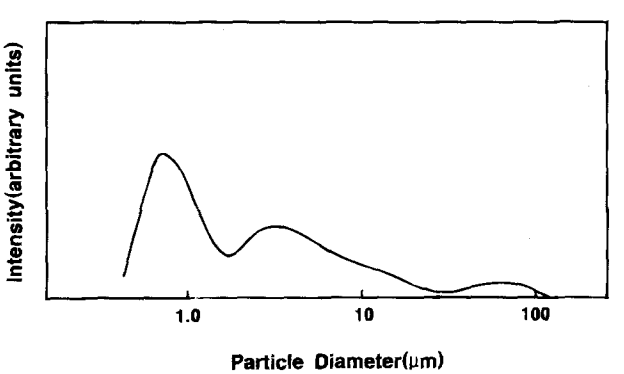

Fig. 1. Particle size distribution of the $La_{0.9}Sr_{0.1}MnO_3$ powder.

* Electrochemical Society Active Member.
[a] Present address: Institute for Inorganic Chemistry, University of Münster, D-48149 Münster, Germany.

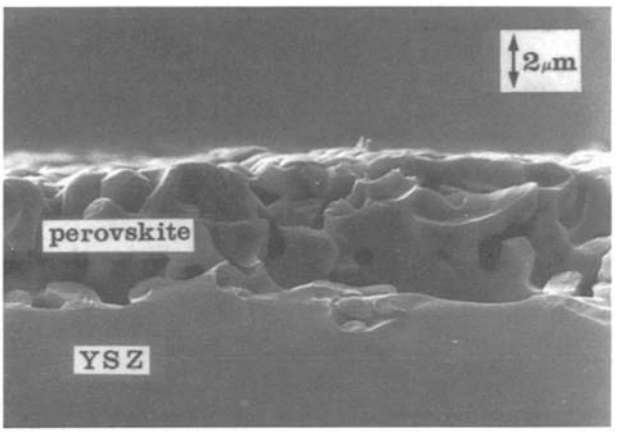

Fig. 2. SEM photograph showing the interfacial region between $La_{0.9}Sr_{0.1}MnO_3$/YSZ.

electrode configuration. Only the half-cell characteristics of the cathode were investigated. The oxygen partial pressure in both sides of the cell was the same. Experiments were performed under 10^{-4} to 1 atm of P_{O_2}, and the measured temperature was in the range of 700 to 900°C.

AC impedance measurements were made over the frequency range of 0.05 Hz to 100 kHz using EG&G PARC 173 potentiostat, 276 interface, and 5208 two-phase lock-in analyzer. Deconvolution of the complex impedance spectra was performed with EG&G PARC 378 electrochemical impedance software. Cyclic voltammetry was performed with the same potentiostat, 175 function generator, and 276 interface. The scan rate was 0.05 mV/s.

XPS measurements.—XPS measurements have been done in a multianalysis ultrahigh vacuum (UHV) chamber equipped with a Leybold-Heraeus spectrometer, electron energy analyzer (HA 150, VSW), and x-ray source (Al kα 1486.6 eV, VSW). The binding energy was calibrated in reference to Ag 3d level.

The electrolyte was 10 m/o yttria-stabilized zirconia (100)-oriented single-crystal plate (1 × 1 × 0.05 cm). The perovskite electrode was deposited by first slurry coating and then calcination at 1200°C for 2 h. As the counterelectrode, Pd/PdO was applied on the other side of the zirconia plate. It was prepared by the slurry coating of Pd paste, followed by heat-treatment at 800°C for 1 h. The scanning electron micrograph (SEM) photograph of the side view of the electrode/electrolyte interface is presented in Fig. 2. The porous electrode layer adhered well to the electrolyte, and the layer thickness is about 5 μm. The resulting cell, having a two-electrode configuration, was mounted on a resistively heated Pt foil with a homemade cell holder.[14]

To obtain the fully oxidized sample of the electrode material, it was anodically polarized at 0.8 V (*vs.* Pd/PdO reference electrode) under 20 mbar of O_2 at 650°C for 30 min and then cooled to room temperature in the same atmosphere. After this treatment, the sample was transferred to the UHV chamber, and the XPS spectrum was obtained (for the spectrum indicated as 0.8 V, 25°C in Fig. 5). Next, the sample was heated to 650°C in the UHV chamber, and a given potential was applied for 2 h. XPS measurements were carried out under the applied potential at this temperature (for the other spectra in Fig. 5). The applied potential was changed to be more cathodic in steps. The electrode layer was so conductive that any charging effects were not observed in the spectra.

Results and Discussion

Cathodic polarization effect.—Figure 3a shows the ac impedance spectra obtained after imposing cathodic potentials for 2 h. The best deconvolution was achieved with the equivalent circuit of $R_1(R_2Q_2)$ (R_3Q_3) as illustrated in Fig. 3b, where a fitted spectrum is also presented with the observed one. Table I summarizes the resulting ac impedance parameters obtained by fitting the spectra of

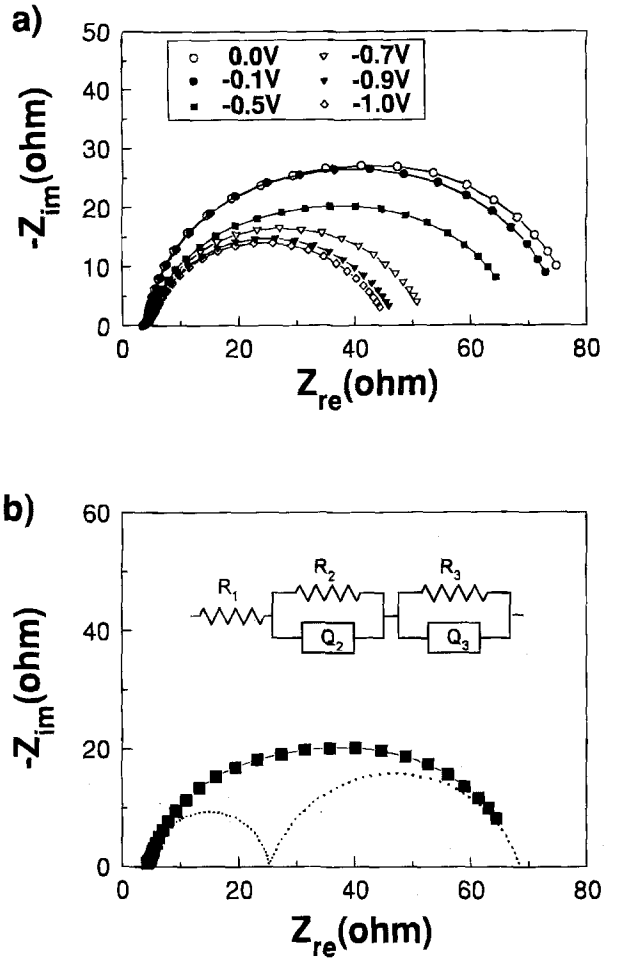

Fig. 3. (a) Evolution of the impedance spectra as a function of applied potential. Each potential was imposed until the spectrum showed a steady value (about 2 h). T = 800°C, P_{O_2} = 0.2 atm. (b) Deconvolution of the impedance spectrum with the equivalent circuit.

Fig. 3a. R_1 was assigned to the ohmic resistance of the electrolyte, R_2Q_2, the parallel combination of the resistance and constant-phase element of impurities or new phases at the electrode/electrolyte interface.[15,18] R_3Q_3 was assigned to the parallel combination of the charge-transfer resistance (R_{ct}) for oxygen reduction and the constant-phase element. The semicircle corresponding to the R_2Q_2 appeared at higher frequency range.

The $1/R_{ct}$ values calculated from the spectra of Fig. 3a are plotted against the applied potentials in Fig. 4. Clearly, the $1/R_{ct}$ values become larger, *i.e.*, electrochemical O_2 reduction rate becomes faster, as the imposed potential is more cathodic. It is of value for later discussion to note that the $1/R_{ct}$ *vs.* potential profile shows a sharp increase

Table I. The fitted ac impedance parameters obtained from the spectra of Fig. 3.

Potential (V)	R_1 (Ω)	R_2 (Ω)	Q_2[a] Y_o (Ω^{-1})	Q_2[a] n	R_3 (Ω)	Q_3[a] Y_o (Ω^{-1})	Q_3[a] n
0.0	3.4	19.2	2.81×10^{-3}	1.00	55.5	5.27×10^{-3}	0.87
−0.1	3.4	19.3	3.00×10^{-3}	1.00	54.9	5.12×10^{-3}	0.85
−0.5	3.5	19.5	2.62×10^{-3}	0.90	44.0	6.77×10^{-3}	0.80
−0.7	3.5	21.5	2.60×10^{-3}	0.89	29.6	7.98×10^{-3}	0.81
−0.9	3.5	16.3	3.29×10^{-3}	0.89	28.3	6.79×10^{-3}	0.77
−1.0	3.5	12.9	3.68×10^{-3}	0.89	28.0	5.95×10^{-3}	0.76

[a] Q is a circuit description code (CDC) to represent the constant-phase element (CPE). [16] Representation of the CPE in admittance is $Y(\omega) = Y_o (j\omega)^n$.

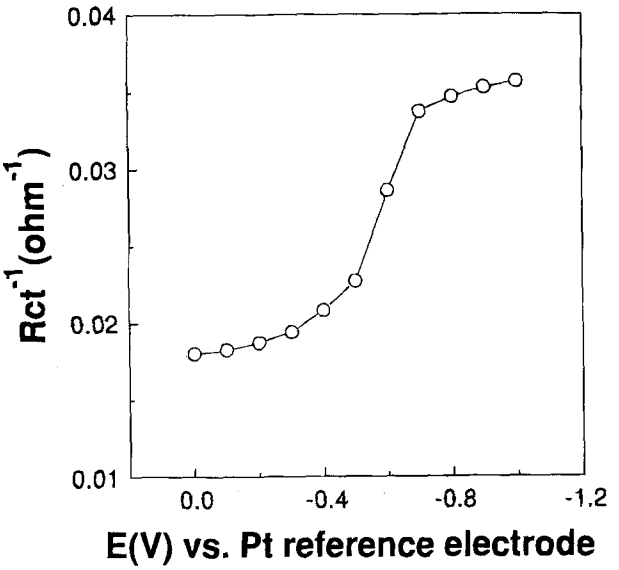

Fig. 4. Plot of $1/R_{ct}$ vs. applied potential. The R_{ct} values were obtained from the spectra of Fig. 3.

around −0.6 V to reach a maximum value at more negative potentials.

The electrolyte resistances (R_1 values) are also listed in Table I. In general, the electrolyte resistance is inversely proportional to the contact area at the electrode/electrolyte interface

$$R_1 = \frac{1}{\sigma} \cdot \frac{l}{A}$$

where R_1, l, and σ mean the resistance, thickness, and conductivity of the electrolyte, respectively. The parameter A indicates the contact area. If the contact area (that is, the three-phase boundary lines) is enlarged by the cathodic polarization, R_1 should be decreased since the l and σ values are invariant under the present experimental condition. However, in our result, the variation in the electrolyte resistances is negligible compared to the large enhancement in $1/R_{ct}$ values. This result tells that the rate enhancement upon cathodic polarization is due to a favorable effect given on the electrode material itself.

To see how the cathodic polarization affects the physicochemical properties of the electrode material itself, *in situ* XPS measurements were performed under UHV condition. Al Kα excited Mn $2p_{3/2}$ and $2p_{1/2}$ spectral region is presented in Fig. 5. Those spectra were corrected by inelastic background and satellites subtraction. Also, the intensity ratios between the elements are listed in Table II. They were weighted by ionization cross section and electron mean free paths.[17,18]

Two features in the Mn 2p spectra are noticeable. First, the peaks are shifted to the lower binding energy side as the applied potential becomes more cathodic. Even though the peak shift is quite small, which is not unusual with Mn 2p bands, a steady shift can be recognized in the figure. In fact, it is known that the binding energy difference between Mn ions of different oxidation states is small (1 to 2 eV).[20] Second, the ionization peaks are broad and do not show any significant line broadening or peak separation as the applied potential or temperature is varied. The first feature, *i.e.*, the binding energy shift, manifests itself in the Mn ions are electrochemically reduced when the electrode is cathodically polarized. If this occurred, the lattice or interstitial oxide ions should be removed from the electrode material for charge compensation.

Cathodic reaction

$$2Mn^{3+} + O^{2-}\ (\text{interstitial}) + 2e^- \rightarrow 2Mn^{2+} + V\ (\text{interstitial}) + O^{2-}\ (\text{electrolyte})$$

$$2Mn^{3+} + O^{2-}\ (\text{lattice}) + 2e^- \rightarrow 2Mn^{2+} + V\ (\text{lattice}) + O^{2-}\ (\text{electrolyte})$$

Anodic reaction

$$O^{2-}\ (\text{electrolyte}) \rightarrow 1/2\ O_2\ (\text{gas}) + 2e^-$$

Overall reaction

$$2Mn^{3+} + O^{2-}\ (\text{interstitial}) \rightarrow 2Mn^{2+} + V\ (\text{interstitial}) + 1/2\ O_2\ (\text{gas})$$

$$2Mn^{3+} + O^{2-}\ (\text{lattice}) \rightarrow 2Mn^{2+} + V\ (\text{lattice}) + 1/2\ O_2\ (\text{gas})$$

In the above scheme, V indicates the oxide vacancies in the interstitial or lattice sites. Actually, Table II indicates that the surface oxygen concentration gradually decreases with increasing cathodic polarization. The anodically polarized (*i.e.*, electrochemically oxidized) sample shows an oxygen excess in stoichiometry ($I_O/(I_{Sr} + I_{La}) = 3.32$). But the cathodically polarized electrodes show an oxygen deficiency ($I_O/(I_{Sr} + I_{La}) < 3.0$), that is, oxide vacancies in the lattice. Also, considering the detection depth for x-ray photoelectron spectroscopy (XPS), these results manifest that the Mn ion reduction/oxide removal even takes place at the external surface of the electrode. It is believed that this electrochemical reaction starts at the electrode/electrolyte interface at the initial stage and propagates to the whole internal and external surface through the grain boundary path in the porous electrode. Mn ions are electrochemically reduced, and O^{2-} ions (the lattice or interstitial oxides) are transported to the electrolyte. At the anode, O^{2-} ions are electrochemically oxidized to produce molecular oxygen. A pressure buildup inside the UHV chamber observed during the cathodic polarization is believed to be due to oxygen evolution. The second feature, *i.e.*, the lack of a fine structure, cannot clearly be explained. This would be possible if the electron exchange (hopping) rates between the Mn ions are faster than the inverse of the XPS time scale (10^{18} s^{-1}).[19]

In short, the XPS data illustrate that under cathodic polarization the Mn ions are reduced and concomitantly oxide vacancies are formed on the electrode surface. However, there is still no indication whether the Mn ion reduction/oxide vacancy formation actually takes place under oxygen atmosphere (not under UHV condition) and whether the surface oxide vacancies participate in the oxygen reduction reaction.

Active reaction sites.—Figure 6 shows the cyclic voltammograms traced with $La_{0.9}Sr_{0.1}MnO_3$ at various O_2 pressures. The potential was moved from 0.0 V to the negative direction, switched at −1.0 V, and scanned to +0.4 V. It can be seen that the reverse currents are larger than the forward ones (hysteresis) on the cathodic current[6] and the hysteresis gradually diminishes as the O_2 pressure is lowered. Furthermore, under nitrogen atmosphere, the hysteresis is not observed (Fig. 7a).

In Fig. 7a, during the forward (negative) scan, the current starts to evolve from −0.5 V to reach a steady value at −1.0 V. On the reverse scan, there appears a current peak at about −0.6 V and another current peak develops from 0.0 V. The cathodic current evolved between −0.6 and −1.0 V can be assigned to either a small electronic conduction of the electrolyte, electrochemical reduction of the trace amount of adsorbed oxygen, or electrochemical reduction of the electrode material. To test the first possibility, a cyclic voltammogram for Pt gauze/YSZ/Pt cell was traced under the same condition as for $La_{0.9}Sr_{0.1}MnO_3$/YSZ/Pt (Fig. 7b). For this experiment, a piece of Pt gauze was contacted, as a working electrode, on the YSZ surface by pressing with an alumina tube. The cyclic voltammogram observed with the Pt gauze electrode does not show any current peaks between 0.2 and −1.3 V. If the current observed in Fig. 7a originated from the electrolyte, the same voltammogram should be traced with the Pt gauze/YSZ/Pt cell. Thus, the first possibility can be excluded. Meanwhile, the voltam-

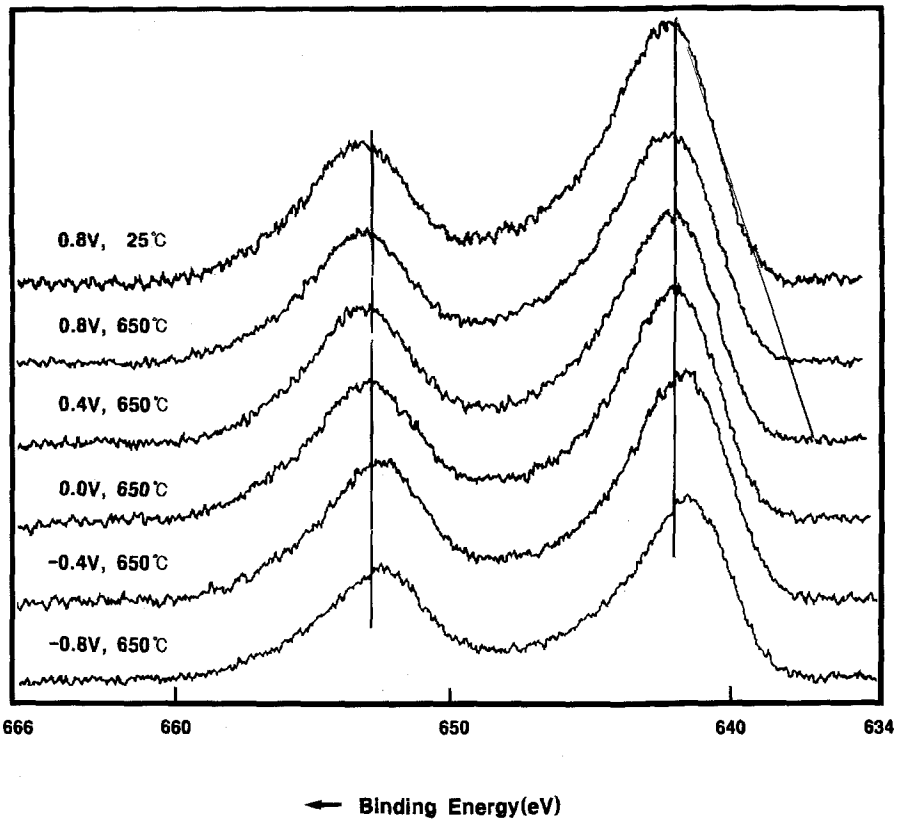

Fig. 5. The Mn $2p_{3/2}$ and $2p_{1/2}$ regions of the Al kα-excited XPS spectra for $La_{0.9}Sr_{0.1}MnO_3$ at various applied potentials. For the top spectrum (0.8 V, 25°C), the sample was pretreated under 20 mbar of O_2 and 0.8 V in the prechamber and transferred to the UHV chamber. For the other spectra, the sample was pretreated at each potential for 2 h in the UHV chamber.

mogram in Fig. 7b suggests that YSZ can be electrochemically oxidized (more positive than about 0.2 V) and reduced (more negative than −1.3 V). A similar result has been reported by Kleitz *et al.*,[20] who proposed that under this extremely polarized condition YSZ can have a mixed conductivity such that oxygen reduction can take place on the YSZ surface.

One of the alternatives, electrochemical reduction of the adsorbed oxygen, can also be discarded as follows. The current values on the forward scans in Fig. 6 are sampled at four different potentials and are plotted against the oxygen pressure (Fig. 8). The sampled currents at −0.3 and −0.6 V show a gradual decrease as the oxygen pressure is lowered. Those sampled at −0.8 and −1.0 V show a similar behavior at higher O_2 pressure but, interestingly, they grow up again below 0.1 atm. This current rise at the lower oxygen pressure on the −0.8 and −1.0 V profiles cannot simply be attributed to oxygen reduction. If only oxygen reduction is involved, the profile should show a steady decrease even under 0.1 atm and eventually the current should approach to zero under N_2 atmosphere. It is, thus, clear that there must be some other electrochemical reduction process involved at −0.8 and −1.0 V. This would be the electrochemical reduction of the electrode material, most probably, the Mn ion reduction coupled with a loss of oxygen ions. Pointing this view to the voltammogram obtained under N_2 condition (Fig. 7a), the cathodic current observed at more negative potential than −0.6 V can be assigned to the Mn ion reduction. In addition, the data in Fig. 7a and 8 demonstrate that the Mn ion reduction/oxide vacancy formation actually takes place even under O_2 atmosphere when the electrode is cathodically polarized (more negative than −0.5 to −0.6 V). It is likely that the Mn ion reduction and O_2 reduction are competing with each other under O_2 atmo-

Table II. The intensity ratio between the elements in $La_{0.9}Sr_{0.1}MnO_3$ with different applied potential.

Potential (V)	(Temp., °C)	I_{Sr}/I_{La}	$I_o/(I_{Sr} + I_{La})$
0.8	(25)	0.13	3.32
0.8	(650)	0.12	2.86
0.4	(650)	0.11	2.79
0.0	(650)	0.10	2.67
−0.4	(650)	0.12	2.59
−0.8	(650)	0.10	2.48

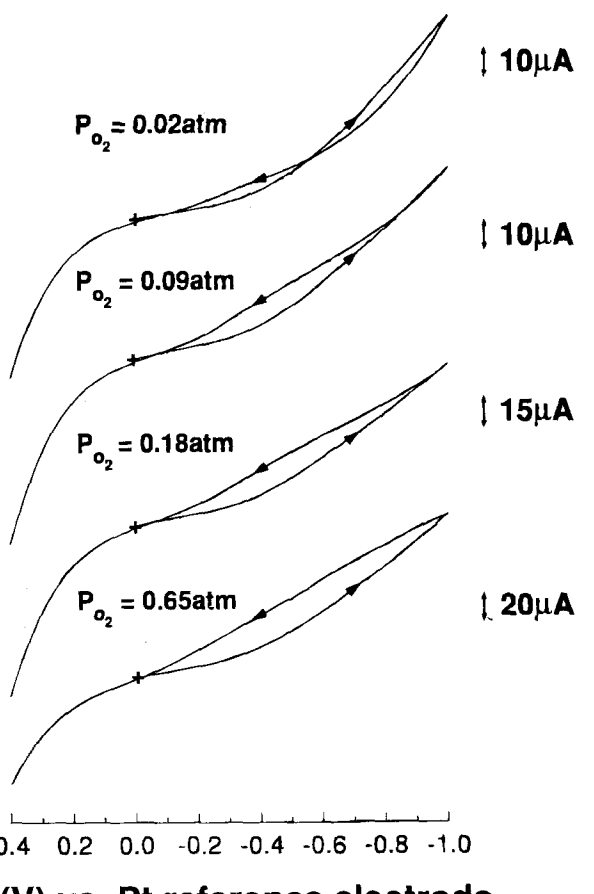

Fig. 6. Cyclic voltammograms traced with $La_{0.9}Sr_{0.1}MnO_3$/YSZ/Pt at various oxygen pressures. T = 700°C, scan rate = 0.05 mV/s.

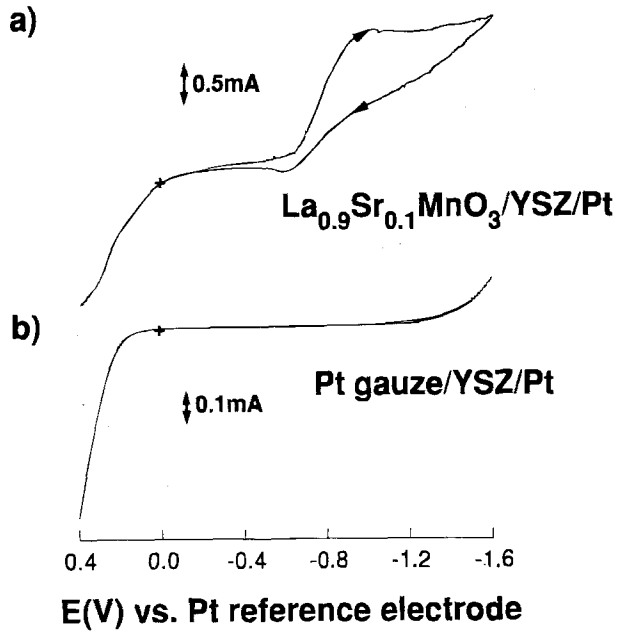

Fig. 7. Cyclic voltammograms traced under N_2 atmosphere. (a) $La_{0.9}Sr_{0.1}MnO_3$/YSZ/Pt, (b) Pt gauze/YSZ/Pt. T = 900°C, scan rate = 0.05 mV/s.

sphere. At high O_2 pressure, O_2 reduction would be dominant, but the reverse would be true at lower pressure.

Now, it is interesting to compare the evolution of $1/R_{ct}$ *vs.* potential (Fig. 4) with the cathodic forward current *vs.* potential in Fig. 7a. They show similar profiles against the potential. If one assumes that the rate-determining step for oxygen reduction on this material is the charge-transfer process (details to be published elsewhere) and that the surface oxide vacancies are active for oxygen reduction, the $1/R_{ct}$ values can be directly related to the amount of surface oxide vacancies. Thus, the enhancement of O_2 reduction rates, which were observed with those electrodes cathodically polarized at more negative potential than −0.5 V, can be ascribed to the enlargement of the surface sites. Figure 7a tells us that the surface oxide vacancy formation is more pronounced at this potential range (more negative than −0.6 V).

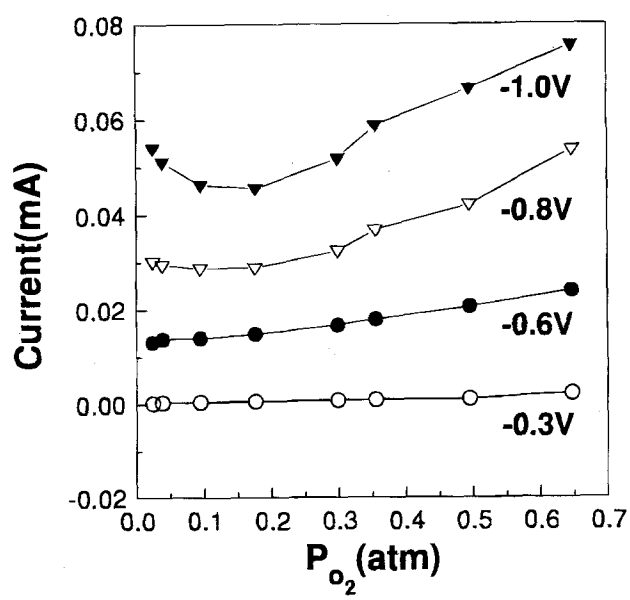

Fig. 8. Plot of the sampled currents *vs.* P_{O_2} The currents were sampled at four different potentials from the voltammograms shown in Fig. 6.

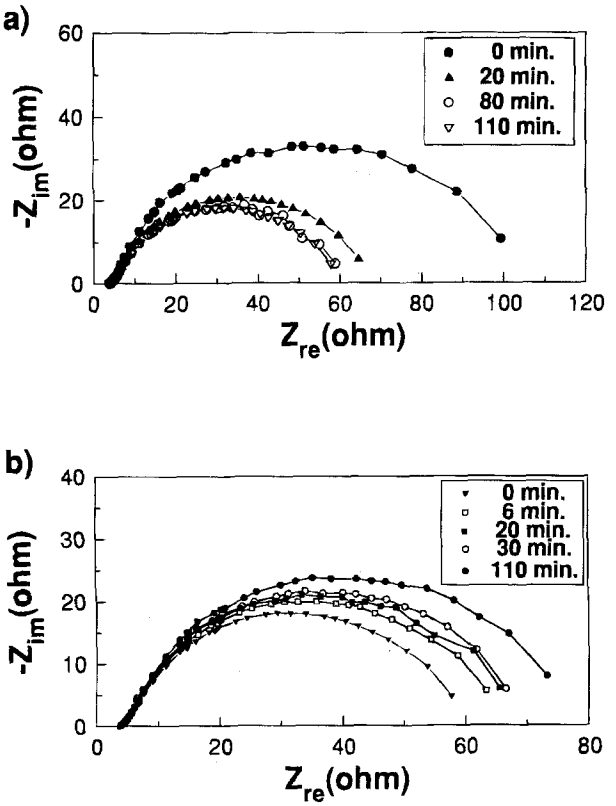

Fig. 9. (a) Evolution of the impedance spectra according to the elapsed time after imposing a potential (−0.5 V). T = 800°C. (b) Evolution of the impedance spectra according to the elapsed time after removing the potential. T = 800°C.

The P_{O_2}-dependent hysteresis phenomena in Fig. 6 shed light on the active sites for O_2 reduction. During the potential cycling, as the potential moves to the negative direction, surface oxide vacancies are formed such that more active sites are exposed to molecular oxygen. As a result, during the reverse scan from −1.0 to 0.0 V, more oxygen molecules would be electrochemically reduced (hysteresis). Intuitively, however, it can be imagined that the three-phase boundary sites are the better reaction sites than the surface sites since O^{2-} ions produced at the latter sites need additional transport processes to move to the electrolyte. For this process, the major transport pathway would be the surface diffusion or grain-boundary diffusion since the bulk diffusion of oxide ions in this electrode material is very slow.[12] At high O_2 pressure, O_2 reduction would take place on the surface sites as well as the three-phase boundary sites since the latter sites are well occupied by oxygen, resulting in a rather significant hysteresis in the reduction current. However, at lower O_2 pressure, the chance for the surface sites to participate in the O_2 reduction would be rather low such that major reaction would take place at the three phase boundary sites. Then, the hysteresis phenomena will gradually disappear as the O_2 pressure is lowered.

Kinetics of the oxide-vacancy formation.—Figure 9 shows the time-dependent impedance spectra which were obtained after imposing (Fig. 9a) and removing (Fig. 9b) a cathodic potential. The initial spectrum in Fig. 9b corresponds to the final spectrum in Fig. 9a. The time-dependent $1/R_{ct}$ profiles are plotted in Fig. 10. It can be seen in the figure that the R_{ct} values keep decreasing under cathodic polarization to reach a steady value. After removal of the applied potential they increase again to reach a certain final value. Evidently, they do not fully recover to the initial value (that before the cathodic polarization). The $1/R_{ct}$ values show a linear relation with $(\text{time})^{1/2}$ at the earlier stage of polarization,[21] but at the later stage the relationship is rather obscure. As discussed above, the observed

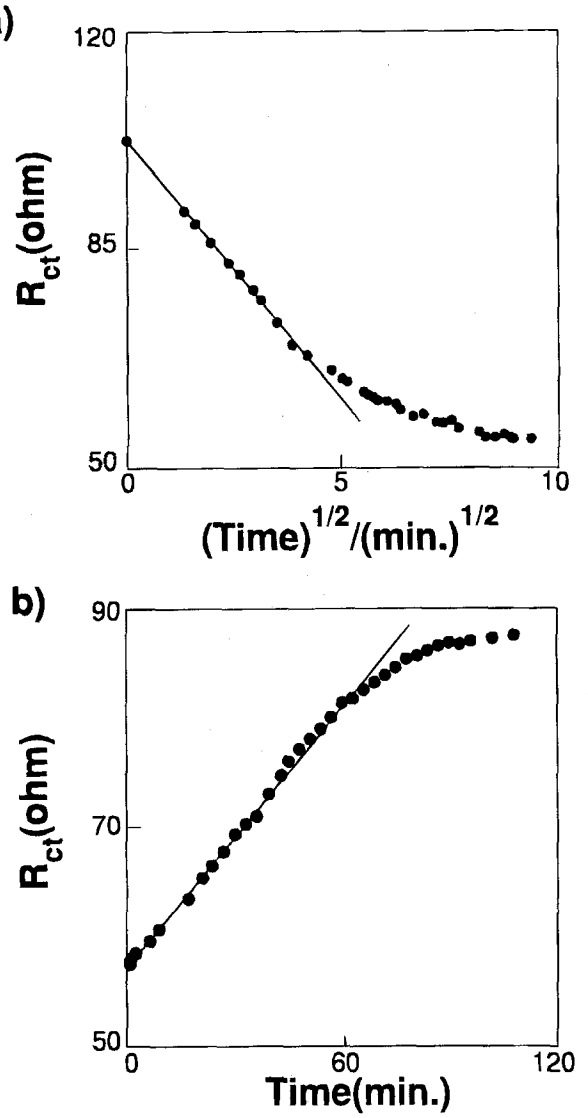

Fig. 10. (a) Plot of R_{ct} vs. (time)$^{1/2}$. The R_{ct} values were obtained from the spectra in Fig. 9a. (b) Plot of R_{ct} vs. time. The R_{ct} values were obtained from the spectra in Fig. 9b.

$1/R_{ct}$ values can be directly related to the amount of surface oxide vacancies. The $t^{1/2}$-dependence of $1/R_{ct}$ (that is, the amount of surface oxide vacancies) suggests that oxide vacancy formation or the removal of the interstitial oxide ions is controlled by diffusional processes. It is likely that under a cathodic polarization Mn ions are electrochemically reduced and oxide ions (lattice oxygen or interstitial oxygen) are transported to the electrolyte for charge compensation. This paired process would start at the electrode/electrolyte interface at the initial stage and propagates to the whole electrode surface through the grain boundary path. The diffusional processes through the grain boundary region seem to be rate limiting since the O^{2-} bulk diffusion in the manganites is very slow.[12] But the kinetics at the later stage cannot be clearly identified. Furthermore, the kinetics of the reverse process, the lattice or interstitial oxide formation looks rather different (Fig. 10). The best fitting was obtained with $1/R_{ct}$ *vs.* time.

Finally, the result that the R_{ct} value does not fully recover to the original value after removing the applied potential suggests that the process of vacancy formation/reoccupation by oxide ions is not fully reversible. Thus, the possibility that cathodic polarization induces a structural change should be considered.

Conclusion

1. Mn ions in $La_{0.9}Sr_{0.1}MnO_3$ are reduced and concomitantly oxide vacancies are formed when the electrode materials are cathodically polarized.

2. Surface oxide vacancy sites as well as the three-phase boundary sites are active in oxygen reduction. But the latter is favored since additional diffusional processes are required for the former sites. At lower O_2 pressure, the three-phase boundaries are the major reaction sites, but the contribution from the surface sites becomes more important at higher O_2 pressure.

Acknowledgment

Funding for this work was provided by the R&D Management Center for Energy and Resources (Korea). S. M. Oh gratefully acknowledges the financial support from the Alexander von Humboldt Foundation.

Manuscript submitted Feb. 1, 1995; revised manuscript received April 21, 1995.

Seoul National University assisted in meeting the publication costs of this article.

REFERENCES

1. K. A. Murugesamoorthi, S. Srinivasan, and A. J. Appleby, in *Fuel Cell Systems,* L. J. M. J. Blomen and M. N. Mugerwa, Editors, pp. 465-473, Plenum Press, New York (1993).
2. A. Hammou, in *Advances in Electrochemical Science and Engineering,* H. Gerischer and C. W. Tobias, Editors, pp. 87-140, VCH Publishers, New York (1992).
3. H. U. Anderson, *Solid State Ion.,* **52,** 33 (1992).
4. Y. Takeda, R. Kanno, M. Noda, Y. Tomida, and O. Yamamoto, *This Journal,* **134,** 2656 (1987).
5. A. Hammouche, E. Siebert, and A. Hammou, *Mater. Res. Bull.,* **24,** 367 (1989).
6. A. Hammouche, E. Siebert, A. Hammou, M. Kleitz, and A. Caneiro, *This Journal,* **138,** 1212 (1991).
7. J. Mizusaki, H. Tagawa, K. Tsuneyoshi, and A. Sawata, *ibid.,* **138,** 1867 (1991).
8. L. G. J. de Haart, R. A. Kuipers, K. J. de Vries, and A. J. Burggraaf, *ibid.,* **138,** 1970 (1991).
9. H. U. Anderson, J. H. Kuo, and M. D. Sparlin, in *Proceedings of First International Symposium on Solid Oxide Fuel Cells,* S. C. Singhal, Editor, PV 89-11, p. 111, The Electrochemical Society Proceedings Series, Pennington, NJ (1989).
10. J. H. Kuo, H. U. Anderson, and D. M. Sparlin, *J. Solid State Chem.,* **83,** 52 (1989).
11. S. Otoshi, H. Sasaki, H. Ohnishi, M. Hase, K. Ishimaru, M. Ippommatsu, T. Higuchi, M. Miyyama, and H. Yanagida, *This Journal,* **138,** 1519 (1991).
12. S. Carter, A. Selcuk, R. J. Chater, J. Kajda, A. Kilkner, and B. C. H. Steele, *Solid State Ionics,* **53-56,** 597 (1992).
13. F. H. van Heuveln, F. P. F. van Berkel, and J. P. P. Huijsmans, in *Proceedings of 14th Risø International Symposium on Material Science,* F. W. Poulsen, J. J. Bentzen, T. Jacobsen, E. Skou, and M. J. L. Østergård, Editors, p. 53, Risø National Laboratory, Roskilde, Denmark (1993).
14. H.-D. Wiemhöfer, *Ber. Bunsenges. Phys. Chem.,* **97,** 461 (1993).
15. J. E. Bauerle, *J. Phys. Chem. Solids,* **30,** 2657 (1969).
16. J. R. Macdonald and W. B. Johnson, in *Impedance Spectroscopy Emphasizing Solid Materials and Systems,* J. R. Macdonald, Editor, pp. 215-238, John Wiley & Sons, Inc., New York (1987).
17. J. H. Scofield, *J. Electron Spectrosc. Relat. Phenom.,* **8,** 129 (1976).
18. D. R. Penn, *ibid.,* **9,** 29 (1976).
19. R. S. Drago, *Physical Methods for Chemists,* 2nd ed., p. 98, Saunders College Publishing, New York (1992).
20. M. Kleitz, T. Kloidt, and L. Dessemond, in *Proceedings of 14th Risø International Symposium on Material Science,* F. W. Poulsen, J. J. Bentzen, T. Jacobsen, E. Skou, and M. J. L. Østergård, Editors, pp. 89-116, Risø National Laboratory, Roskilde, Denmark (1993).
21. B. Gharbage, T. Pagnier, and A. Hammou, *This Journal,* **141,** 2118 (1994).